# *Probe Position Planning for Measuring Cylindrical Gears on a Four-Axis CNC Machine*

*Yi-Hui Lee, Jia-Hong Cai, Yi-Pei Shih**

*Department of Mechanical Engineering National Taiwan University of Science and Technology*

*Email: shihyipei@mail.ntust.edu.tw*

*Abstract - During large-size gear manufacturing by form grinding, the actual tooth surfaces will differ from the theoretical tooth surface because of errors in the clamping fixture and machine axes and machining deflection. Therefore, to improve gear precision, the gear tooth deviations should be measured first and the flank correction implemented based on these deviations. To address the difficulty in large-size gear transit, we develop an on-machine scanning measurement for cylindrical gears on the five-axis CNC gear profile grinding machine that can measure the gear tooth deviations on the machine immediately after grinding. Our results can serve as a foundation for follow-up research on closed-loop flank correction technology. This measuring process, which is based on the AGMA standards and measuring processes provided by the Klingelnberg four-axis gear measuring center, includes the (1) profile deviation, (2) helix deviation, (3) pitch deviation, and (4) flank topographic deviation. The mathematical models for measuring probe positioning are derived using the base circle method. We also calculate measuring positions that can serve as a basis for programming the NC codes of the measuring process and verify them using the 3-D virtual reality NC path simulation and collision detection system developed by our lab.*

*Keywords - Four-axis gear measuring center, measuring probe positioning, base circle method.*

## *I. INTRODUCTION*

The newly developed gear profile grinding machines, such as the Höfler RAPID series, the Niles ZP series, and the Luren Precision LFG series, are all Cartesian-type structures with movable axes controlled by computer numerical control (CNC). These machines are specifically designed for grinding spur and helical, external and internal gears using the form grinding method. They not only offer a precise simultaneous five-axis movement that enables free-form grinding but include an NC dressing device for free-form wheel profiles. To improve gear manufacturing precision, a correction is applied according to a measurement that must be made before correction. Usually, to take into account the difficulty in large-size gear transit, the measuring device is integrated into the wheel head and provides an on-machine gear precision evaluation. There are two probing systems for gear measurement, the touch trigger probe and the scanning probe. The latter is speedier and more precise in measurement than the former.

In terms of gear design, Litivin and Fuentes [2] have provided a mathematical model for involute gears and also established a mathematical model for the form grinding method. For gear measurement, the AGMA gear standard [1] clearly defines what is to be measured in cylindrical gears, including the profile, helix, and pitch. Shih and Fong [3] proposed flank correction methodologies based on the CNC hypoid gear generator, and defined the topographic errors for bevel gears. The Klingelnberg operator's manual [4] clearly describes the measuring paths for the profile, helix, and pitch for cylindrical gears, and the measuring path of topographic measurement for bevel gears. Finally, Yuzaki [5] proposed a new method for measuring an involute gear tooth profile by moving the probe along a line of action to enable a shorter measuring path than in the base circle method.

In the domestic gear industry, off-machine measurement is applied after gear manufacturing, but the errors and the time needed for gear loading and unloading reduce gear precision and production efficiency. We therefore develop an on-machine scanning probe measurement for a cylindrical gear on a five-axis CNC gear profile grinding machine. In this paper, we establish the mathematical models for positioning the scanning probe, which could then be used in further work to program the NC codes for the profile, helix, pitch, and flank topographic measurements.

## *II. MEASURING COORDINATE SYSTEMS*

The DOF of the proposed measuring system is arranged based on the modern gear measuring center, which has four numerically closed-loop controlled axes: three rectilinear motions $(C_x, C_y, C_z)$, and one rotational motion $\psi_b$ (see Fig. 1). Such a measuring machine is always a vertical structure whose coordinate systems $S_m$ and $S_1$ are rigidly connected to the program zero and work gear, respectively. Here, $\psi_b$ is the rotation angle of the work gear, and $(C_x, C_y, C_z)$ – coordinates that refer to the measuring program zero – are rectilinear axes for probe positioning.

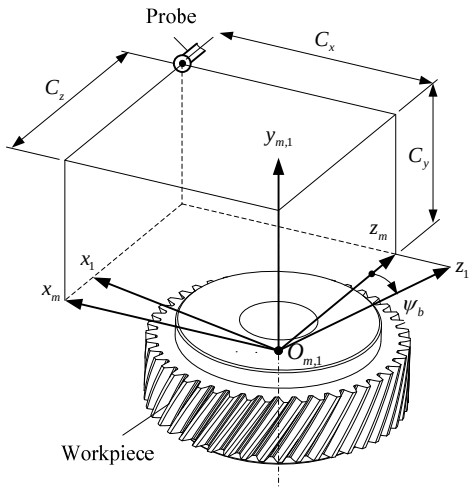


Fig. 1 Measuring coordinate systems.

## III. PROFILE, HELIX AND PITCH MEASUREMENTS

### A. Base Circle Method

Fig. 2 illustrates the measurement of the involute gear using the base circle method. The measuring probe is moved along the X direction, which is tangent to the base circle, while the workpiece axis is rotated simultaneously. Because the directions of the profile normal and the probe movement are the same, the measured displacement is the normal deviation between the actual and theoretical tooth surfaces. The advantage of the base circle method is that the measuring points are always on the fixed point of the probe surface, so that the probe roughness has no effect on the measurement result. This method is therefore popular because of its high accuracy. Here, we use the base circle method to derive the probe positions for the profile, helix, and pitch measurements.

### B. Profile Measurement

The profile deviation is the normal difference from the involute profile. In the scanning measurement, the probe positions and the probe displacements (which differ from the standard involute) are recorded and serve as the normal errors of the profile. First, we must derive the positions of the involute profile in the transverse plane. Then, because the NC measuring path is the path of the probe related to program zero (the workpiece center), we must also derive the positions of the probe center according to the involute profile and the probe radius. As shown in Fig. 3, the related parameters for the profile measuring points are the (1) pitch radius $r_0$, (2) base radius $r_b$, (3) outside radius $r_a$, (4) TIF radius $r_{Tif}$, (5) tooth space angle $\theta_{th}$, (6) number of pitch measuring points $n_p$, and (7) probe radius $r_p$.

Fig. 3 shows the measuring positions for the profile from the TIF to the outside circle, and Fig. 4 (a) defines the involute curve. According to involute theory, the roll angles of start point $\alpha_{rb}$ and end point $\alpha_{re}$ are first derived as shown in (1), and then the roll angle between the start and end points is divided equally to get $n_p$ roll angles for the measuring points.

$$\alpha_{rb} = \cos^{-1}\left(r_b / r_{Tif}\right),\ \alpha_{re} = \cos^{-1}\left(r_b / r_a\right) \qquad (1)$$

Because $O_m cb$ is a right-angled triangle, the line $O_m b$ can be calculated using the base circle radius $r_b$ and the roll angle $\alpha_r$ as in (2). Substituting the roll angle $\alpha_r^{(i)}$ into (2) gives the measuring radius $r_m^{(i)}$ for every measuring point.

$$r_m = r_b / \cos\alpha_r \qquad (2)$$

The translational positions of the profile measuring points are derived in (3), where $\pm$ represents the left and right flank, respectively.

$$\mathbf{r}_m^{(p)}(\alpha_r) = [\pm\sqrt{r_m^2 - r_b^2} \quad 0 \quad r_b \quad 1]^T \qquad (3)$$

Fig. 4 (b) shows that the involute curve is rotated by angle $\Delta\theta_{th}$ so that the tooth space center coincides with the reference point at which $\Delta\theta_{th}$ is the difference in the tooth thickness angle. As shown in Fig. 4 (c), rotating the work piece by angle $-(\theta + \Delta\theta_{th})$ positions the line $bc$ along the same direction as the X axis. As a result, the contact point on the probe surface is always the same, and the deviation measured is the normal error of the profile. The angles of the profile measuring points are derived as in (4), where $\mp$ represents the left and right flank, respectively.

$$b_m^{(p)}(\alpha_r) = \mp(\theta + \Delta\theta_{th}) \qquad (4)$$

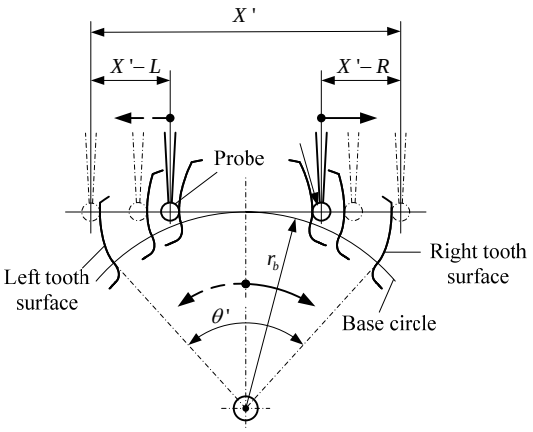


Fig. 2 Base circle method.

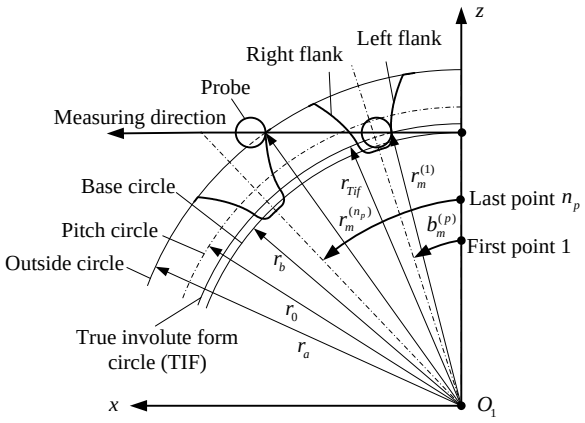


Fig. 3 Profile deviation measurement.

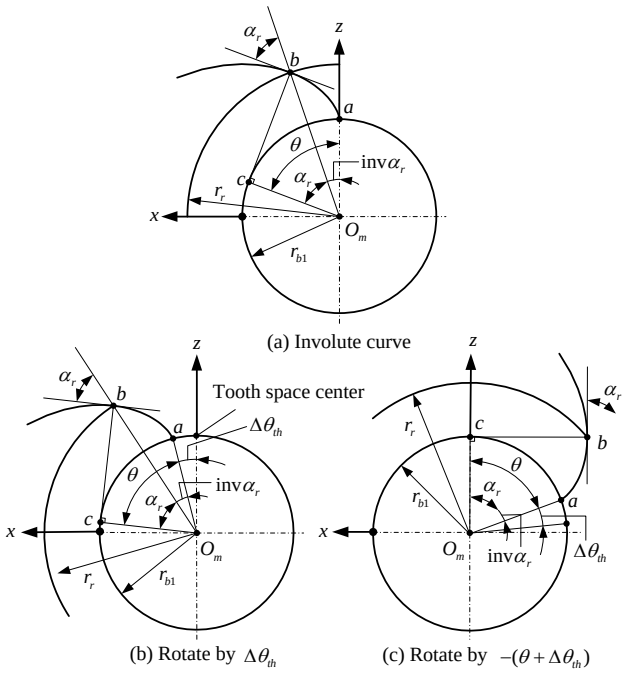


Fig. 4 Definition of involute curve.

where

$$\begin{cases} \theta = \alpha_r + inv(\alpha_r),\ \alpha_{rp} = \cos^{-1}\left(r_b / r_p\right) \\ \Delta\theta_{th} = \theta_{th}/2 - inv(\alpha_{rp}) = \theta_{th}/2 - (\tan\alpha_{rp} - \alpha_{rp}) \end{cases}.$$

The profile measuring NC path is programmed based on the probe center, which is located on the offset of the profile curve with an offset distance $r_p$ as shown as Fig. 5. During profile measurement, the tangent $\mathbf{t}_m^{(p)}$ of the profile curve on the profile point in the transverse plane is always along the Z direction (the measuring coordinate system), and the angle between vector $\mathbf{q}_m^{(p)}$ of $\overline{ML}$ and the transverse plane is equal to the base lead angle. The surface normal $\mathbf{n}_m^{(p)}$ of the profile point in the transverse plane can thus be calculated as follows:

$$\begin{cases} \mathbf{t}_m^{(p)} = \begin{bmatrix} 0 & 0 & 1 \end{bmatrix}^T \\ \mathbf{q}_m^{(p)} = \pm h_d \begin{bmatrix} \cos\lambda_b & \sin\lambda_b & 0 \end{bmatrix}^T \\ \mathbf{n}_m^{(p)} = \mathbf{q}_m^{(p)} \times \mathbf{t}_m^{(p)} = \pm h_d \begin{bmatrix} \sin\lambda_b & -\cos\lambda_b & 0 \end{bmatrix}^T \end{cases} \quad (5)$$

where $\pm$ represents the left and right flank, respectively, and $h_d$ is $\pm 1$ and represents the right-hand and left-hand gears, respectively.

Using the profile position, the surface normal, and the probe radius $r_p$, the probe center can be derived by the following equation:

$$\mathbf{r}_m^{(pp)}(\alpha_r) = \mathbf{r}_m^{(p)} + r_p \mathbf{n}_m^{(p)} = [x_m^{(pp)} \quad y_m^{(pp)} \quad z_m^{(pp)} \quad 1]^T \quad (6)$$

### *C. Helix Measurement*

The helix deviation is the normal difference between the measured and the theoretical helix of the gear. When the deviation is too large, edge contact results that a decline in gear strength. The scanning probe measurement records the probe displacements that differ from the standard gear helix and probe positions, which then serve as the normal errors of the helix.

The principle of the helix measurement is similar to that of the profile measurement, except that only the pitch points along the gear helix direction are measured. The probe center is derived based on the involute helix and the probe radius. As shown in Fig. 6, the related parameters for the helix measuring points are the (1) pitch radius $r_0$, (2) base radius $r_b$, (3) tooth space angle $\theta_{th}$, (4) face width $b$, (5) start position $l_{mb}$, (6) end position $l_{me}$, (7) the number of helix measuring points $n_l$, and (8) probe radius $r_p$.

As also shown in Fig. 6, the start position $l_{mb}$ and end position $l_{me}$ for the helix measurement are first defined by the face width, and then the helix line between the start and end points is divided equally to get $n_l$ positions of the helix measurement. The translational positions of the helix measuring points are derived as in (7), where $\pm$ represents the left and right flank, respectively.

$$\mathbf{r}_m^{(l)}(l_m) = [\pm\sqrt{r_0^2 - r_b^2} \quad l_m \quad r_b \quad 1]^T \quad (7)$$

Once the helix is defined, the gear rotation angle $\theta_l$ for every helix measuring point can be derived as follows:

$$\theta_l(l_m) = l_m / (r_0 \cot\beta) \quad (8)$$

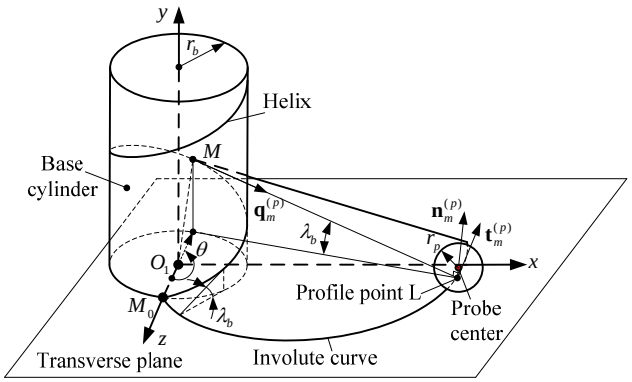


Fig. 5 Generation of involute helix surface.

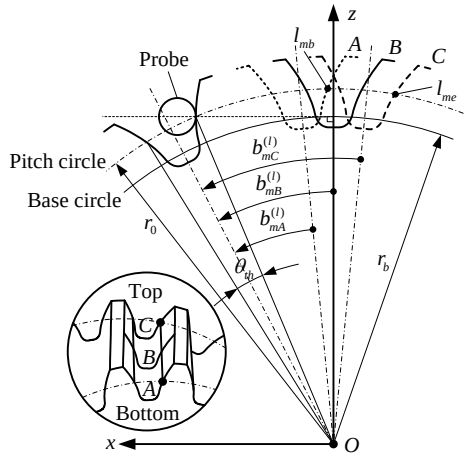


Fig. 6 Lead deviation measurement.

The angles of the helix measuring points are derived as in (9), where $\mp$ represents the left and right tooth flank, respectively.

$$b_m^{(l)}(l_m) = \theta_l \mp (\alpha_{rp} + inv(\alpha_{rp}) + \Delta\theta_{th}) \quad (9)$$

The helix measuring NC path is programmed based on the probe center, which is located on the offset of the helix curve with an offset distance $r_p$. Using the helix position, the surface normal, and the probe radius $r_p$, the probe center can be derived as in the following equation:

$$\mathbf{r}_m^{(lp)}(l_m) = \mathbf{r}_m^{(l)} + r_p \mathbf{n}_m^{(l)} = [x_m^{(lp)} \quad y_m^{(lp)} \quad z_m^{(lp)} \quad 1]^T \quad (10)$$

### *D. Pitch Measurement*

The pitch deviation is the displacement of the tooth flank from its theoretical position. Because the actual pitch may be larger or smaller than the theoretical pitch, the pitch deviation can have a plus or minus value. When the deviation is too large, it will influence the accuracy and stability of the gear transmission. As shown in Fig. 7, the proposed measuring method is to move the probe center to the zero of the X axis and the specified coordinate of the Y and Z axes. The workpiece is first rotated about the Y axis so that it touches the pitch position of the right flank and then is rotated reversely to touch the pitch point of the left flank. Further calculation is therefore needed of rotation angle B and positions Y and Z.

First, we derive the pitch position in the transverse plane. Because the NC measuring path is the path of the probe center related to the reference point of the workpiece

center, the probe center also needs to be further derived. Lastly, we use geometric constraints to solve the above-mentioned axis positions.

As shown in Fig. 7, the related parameters for the pitch measuring points are the (1) number of teeth $z_1$, (2) pitch radius $r_0$, (3) base radius $r_b$, (4) tooth space angle $\theta_{th}$, and (5) probe radius $r_p$. Assuming that $\mathbf{r}_p$ and $\mathbf{n}_p$ are the position vector and the normal vector of the pitch point that is tangent to the base circle, respectively, these parameters can be derived as in (11), where ± represents the left and right flank, respectively, and $h_d$ represents the hand direction:

$$\begin{cases} \mathbf{r}_p = \begin{bmatrix} \pm r_0 \sin\alpha_{rp} & 0 & r_b & 1 \end{bmatrix}^T \\ \mathbf{n}_p = \pm h_d \begin{bmatrix} \sin\lambda_b & -\cos\lambda_b & 0 \end{bmatrix}^T \end{cases} \tag{11}$$

Rotating the workpiece about the Y axis by angle $\theta_p$ makes the probe touch the pitch point of the tooth flank. The position vector $\mathbf{r}_m^{(i)}(\theta_p)$ and the unit normal vector $\mathbf{n}_m^{(i)}(\theta_p)$ of the measuring flank pitch point can then be calculated as follows:

$$\begin{cases} \mathbf{r}_m^{(i)}(\theta_p) = \mathbf{M}_{mp}(\theta_p)\mathbf{r}_p \\ \mathbf{n}_m^{(i)}(\theta_p) = \mathbf{L}_{mp}(\theta_p)\mathbf{n}_p \end{cases} \tag{12}$$

where

$$\mathbf{M}_{mp}(\theta_p) = \begin{bmatrix} \cos\theta_p & 0 & -\sin\theta_p & 0 \\ 0 & 1 & 0 & 0 \\ \sin\theta_p & 0 & \cos\theta_p & 0 \\ 0 & 0 & 0 & 1 \end{bmatrix}.$$

and the rotation matrix $\mathbf{L}_{mp}$ is the $3\times3$ matrix of $\mathbf{M}_{mp}$.

Using the pitch position, the surface normal of the pitch point, and the probe radius $r_p$, we can derive the probe center as in (13), where ± represents the left and right flank, respectively, and $h_d$ equals plus or minus and represents the right-hand and left-hand gears, respectively.

$$\begin{aligned} \mathbf{r}_m^{(ip)}(\theta_p) &= \mathbf{r}_m^{(i)}(\theta_p) + r_p\mathbf{n}_m^{(i)} \\ &= [x_m^{(ip)} \quad y_m^{(ip)} \quad z_m^{(ip)} \quad 1]^T \end{aligned} \tag{13}$$

where

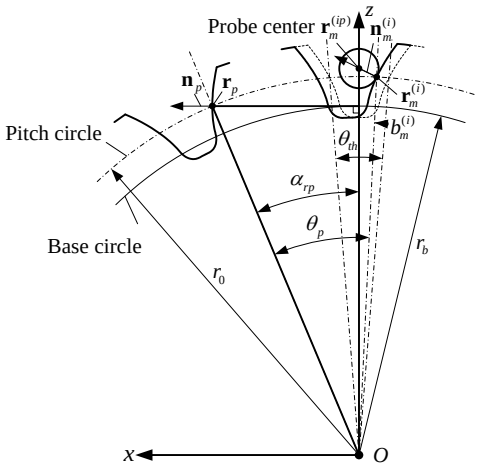

Fig. 7 Pitch deviation measurement.

$$\begin{cases} x_m^{(ip)}(\theta_p) = \pm\cos\theta_p\left(h_d r_p \sin\lambda_b + r_0 \sin\alpha_{rp}\right) - r_b\sin\theta_p \\ y_m^{(ip)}(\theta_p) = \pm\left(-h_d r_p \cos\lambda_b\right) \\ z_m^{(ip)}(\theta_p) = \pm\sin\theta_p\left(h_d r_p \sin\lambda_b + r_0 \sin\alpha_{rp}\right) + r_b\cos\theta_p \end{cases}.$$

During the pitch measurement, the probe center lies on the Y-Z plan, i.e. $x_m^{(ip)} = 0$, so the rotation angle $\theta_p$ can be solved as in (14), where ± represents the left and right flank, respectively.

$$\theta_p = \pm\cos^{-1}\left(\frac{r_b}{\sqrt{\left(r_p\sin\lambda_b + h_d r_0\sin\alpha_{rp}\right)^2 + r_b^2}}\right) \tag{14}$$

Substituting $\theta_p$ into (13) gives the probe center position $\mathbf{r}_m^{(ip)}$, so the rotation angle of workpiece $b_m^{(i)}$ can be calculated by (15), where ± represents the left and right flank, respectively. Because all the teeth must be measured during the pitch measurement, the workpiece is rotated by $b_m^{(i)} + 2\pi k / z_1$, where $k$ is the measuring teeth indexing.

$$b_m^{(i)} = \pm\left(\theta_{th}/2 + \alpha_{rp}\right) - \theta_p \tag{15}$$

## *III. TOPOGRAPHIC MEASUREMENT*

Form grinding is the most popular finishing process for large-size gears because of its high accuracy, efficiency, and flexibility in tooth flank modification. In gear design, topographic modification is applied to the tooth flank using loaded tooth contact analysis (LTCA), which takes into account the gear tooth, shaft, and housing deflections. Therefore gear surface need to be modified on the flank topographically. In gear manufacturing, the tooth flank deviations are composed of the profile and helix deviations. That also caused topographic errors. Accordingly, recent research has developed a topographic correction that eliminates above-mentioned topographic errors. In this paper, we derive the probe center for the topographic measurement by measuring the bevel gear.

The related parameters (Fig. 8) for the flank topographic measurement are the (1) outside radius $r_a$, (2) root radius $r_f$, (3) face width $b$, (4) probe radius $r_p$, and (5) number of columns (face width) $n_c$ and number of rows (tooth depth) $n_r$. Fig. 9 shows the lattice points on the Y-Z plane. We determine the four apices $\mathbf{P}_{t0} \sim \mathbf{P}_{t3}$ based on the tooth line of the gear blank, and determine the four apices $\mathbf{P}_{e0} \sim \mathbf{P}_{e3}$ by considering the reduction in the measuring area. The number of lattice points is usually $9\times5$ points, i.e. the number of columns is 9, and the number of rows is 5. The coordinates for all lattice points are given as $\mathbf{r}_{pt}^{(i,j)} = (y_{pt}^{(i,j)}, z_{pt}^{(i,j)})$.

Assuming that the position equation of the cylindrical gear is $\mathbf{r}_1(u,\beta)$, the surface normal can be derived according to differential geometry as follows:

$$\mathbf{n}_1(u,\beta) = \frac{\dfrac{d\mathbf{r}_1(u,\beta)}{du}\times\dfrac{d\mathbf{r}_1(u,\beta)}{d\beta}}{\left\|\dfrac{d\mathbf{r}_1(u,\beta)}{du}\times\dfrac{d\mathbf{r}_1(u,\beta)}{d\beta}\right\|} \tag{16}$$

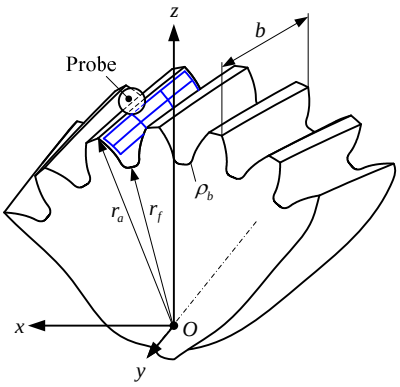


Fig. 8 The flank topographic measurement.

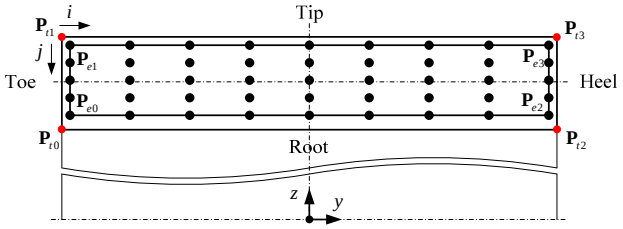


Fig. 9 The plane topographic.

The tooth surface consists of only two variables – $u$ and $\beta$ – which allows the topographic points to be solved through two boundary equations of the gear blank, as in (17). Substituting the determined $u^{(i,j)}$ and $\beta^{(i,j)}$ into $\mathbf{r}_1(u,\beta)$ and (16) gives the topographic points and their surface normal (Fig. 10), respectively.

$$\begin{cases} z_{pt}^{(i,j)} - \sqrt{x_1^2(u,\beta) + z_1^2(u,\beta)} = 0 \\ y_{pt}^{(i,j)} - y_1(u,\beta) = 0 \end{cases} \tag{17}$$

To shorten the measuring distance so that the measuring position is close to the X axis, the theoretical flank topographic is rotated about the Y axis by angle $\theta$ to make the x coordinate of flank point equal to zero. The angle $\theta$ can then be calculated using the following equation:

$$\theta^{(i,j)} = \tan^{-1}\left(x_1^{(i,j)}, z_1^{(i,j)}\right) \tag{18}$$

Substituting (18) into (19) gives the position and surface normal after rotation:

$$\begin{cases} \mathbf{r}_r = \mathbf{M}_{r1}(\theta)\mathbf{r}_1 \\ \mathbf{n}_r = \mathbf{L}_{r1}(\theta)\mathbf{n}_1 \\ b_r = \theta \end{cases} \tag{19}$$

where

$$\mathbf{M}_{r1} = \begin{bmatrix} \cos\theta & 0 & \sin\theta & 0 \\ 0 & 1 & 0 & 0 \\ -\sin\theta & 0 & \cos\theta & 0 \\ 0 & 0 & 0 & 1 \end{bmatrix}.$$

The topographic measuring NC path is programmed based on the probe center, which is located on the offset of the topographic points with an offset distance $r_p$. Using the topographic point, the surface normal, and the probe radius $r_p$, the probe center can be derived as follows:

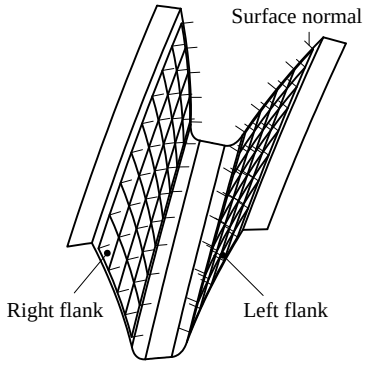


Fig. 10 Topographic points and their surface normal.

$$\begin{cases} \mathbf{r}_r^{(p)} = \mathbf{r}_r + r_p\mathbf{n}_r \\ b_r^{(p)} = b_r \end{cases} \tag{20}$$

After measuring every column of tooth depth points, the probe must be retracted to avoid a collision between it and the tooth flank. The retraction paths are shown as dashed lines in Fig. 11, in which the first path runs from point $(1,n_r)$ to point $(2,1)$. There are $(n_c-1)$ segments, and the number of retracting points in every segment is $n_r$. Here, the retracting points are derived by linear interpolation, in which we also raise the probe by a distance of 0.2 surface normal for safety considerations. The positions of the retracting points are calculated as follows:

$$\begin{aligned} \mathbf{r}_b^{(p)}(i,j) = \mathbf{r}_r^{(p)}(i,n_r) + \frac{\mathbf{r}_r^{(p)}(i+1,1) - \mathbf{r}_r^{(p)}(i,n_r)}{n_r - 1}(j-1) \\ + 0.2\mathbf{n}_r^{(p)}, \quad i = 1 \sim n_c,\ j = 1 \sim n_r \end{aligned} \tag{21}$$

## *III. NUMERICAL EXAMPLES*

To demonstrate the coordinates of the measuring points (the probe center) calculated by the proposed equations, we use an external helical gear as a workpiece. The main parameters of the helical gear are listed in TABLE 1. All coordinates $(x,y,z,b)$ refer to the program zero, which is located on the workpiece center.

TABLE 2 shows the probe center coordinates for profile measurement using the base circle method for both the left and right flanks. The position is measured in millimeters and the angle in degrees.

TABLE 3 presents the probe center coordinates for the helix measurement using the base circle method for both the left and right flanks. The position is measured in millimeters and the angle in degrees.

During the pitch measurement, the probe is moved to the specified coordinates of the X, Y, and Z axes, and the workpiece is rotated about the Y axis by angle B. TABLE 4 lists the probe center coordinates for the pitch measurement for both the left and right flanks. The position is measured in millimeters and the angle in degrees

TABLE 5 shows the probe center coordinates for the flank topographic measurement; however, because these points are so numerous, only 9 flank points, for both left and right flanks, are listed here. The position is measured in millimeters and the angle in degrees.

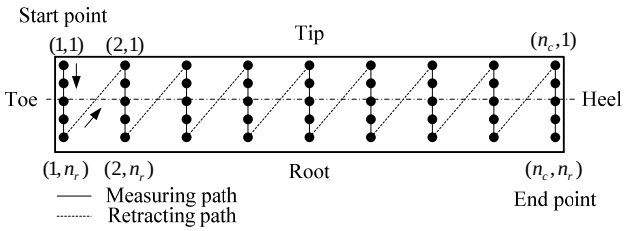

Fig. 11 Retracting path.

## *IV. CONCLUSIONS*

In this paper, we establish mathematical models for measuring point coordinates based on the AGMA standards and measuring processes provided by the Klingelnberg gear measuring center. The measuring process we develop includes the (1) profile deviation, (2) helix deviation, (3) pitch deviation, and (4) flank topographic deviation. The first three are derived using the base circle method, and the last is similar to the bevel gear measurement. All the mathematical models for measuring probe positioning are derived based on the theoretical involute curve.

## *ACKNOWLEDGMENT*

The authors are grateful to the National Science Council of the R.O.C for its financial support. Part of this work was performed under Contract No. NSC 99-2622-E-194-007-CC2.

## *REFERENCES*

[1] ANSI/AGMA 2015-1-A01, *Accuracy Classification System - Tangential Measurements for Cylindrical Gears*, 2002.
[2] Litvin, F. L., Fuentes, A., *Gear Geometry and Applied Theory*, 2nd edition, Cambridge University Press, New York, 2004.
[3] Shih, Y.-P., and Fong, Z.-H., 2008, "Flank Correction for Spiral Bevel and Hypoid Gears on a Six-Axis CNC Hypoid Gear Generator," ASME J. Mech. Des., 130 (6), 062604.
[4] Klingelnberg P40 Operator's Manual, Cylinder Gear Software.
[5] Yuzaki, M., "Method of Measuring an Involute Gear Tooth Profile," US Patent, 2011.

TABLE 1
BASIC PARAMETERS OF THE HELICAL GEAR

| Items | Symbol | Unit | Value |
|---|---|---|---|
| Module | $m_n$ | *mm* | 10.000 |
| Number of teeth | $z_1$ | – | 45 |
| Pressure angle | $\alpha_n$ | deg | 20.000 |
| Spiral angle | $\beta$ | deg | RH, 30.000 |
| Shift coefficient | $x_1$ | – | 0.000 |
| Face width | $b$ | *mm* | 120.000 |
| Diameter of pitch circle | $d_p$ | *mm* | 519.615 |
| Diameter of outside circle | $d_a$ | *mm* | 539.615 |
| Diameter of root circle | $d_f$ | *mm* | 494.615 |
| Diameter of probe | $d_p$ | *mm* | 4.000 |

TABLE 2
COORDINATES OF THE MEASURING POINTS FOR THE PROFILE MEASUREMENT

| | Left flank | | | | Right flank | | | |
|---|---|---|---|---|---|---|---|---|
| NO. | X | Y | Z | B | X | Y | Z | B |
| 1 | 72.713 | -0.940 | 239.514 | -17.688 | -72.713 | 0.940 | 239.514 | 17.688 |
| 2 | 77.703 | -0.940 | 239.514 | -18.881 | -77.703 | 0.940 | 239.514 | 18.881 |
| 3 | 82.754 | -0.940 | 239.514 | -20.090 | -82.754 | 0.940 | 239.514 | 20.090 |
| 4 | 87.871 | -0.940 | 239.514 | -21.314 | -87.871 | 0.940 | 239.514 | 21.314 |
| 5 | 93.058 | -0.940 | 239.514 | -22.554 | -93.058 | 0.940 | 239.514 | 22.554 |
| 6 | 98.321 | -0.940 | 239.514 | -23.813 | -98.321 | 0.940 | 239.514 | 23.813 |
| 7 | 103.665 | -0.940 | 239.514 | -25.092 | -103.665 | 0.940 | 239.514 | 25.092 |
| 8 | 109.097 | -0.940 | 239.514 | -26.391 | -109.097 | 0.940 | 239.514 | 26.391 |
| 9 | 114.622 | -0.940 | 239.514 | -27.713 | -114.622 | 0.940 | 239.514 | 27.713 |
| 10 | 120.247 | -0.940 | 239.514 | -29.059 | -120.247 | 0.940 | 239.514 | 29.059 |
| 11 | 125.979 | -0.940 | 239.514 | -30.430 | -125.979 | 0.940 | 239.514 | 30.430 |

TABLE 3
COORDINATES OF THE MEASURING POINTS FOR THE HELIX MEASUREMENT

| | Left flank | | | | Right flank | | | |
|---|---|---|---|---|---|---|---|---|
| NO. | X | Y | Z | B | X | Y | Z | B |
| 1 | 102.428 | -62.940 | 239.514 | -32.690 | -102.428 | -61.060 | 239.514 | 16.902 |
| 2 | 102.428 | -50.540 | 239.514 | -31.111 | -102.428 | -48.660 | 239.514 | 18.481 |
| 3 | 102.428 | -38.140 | 239.514 | -29.532 | -102.428 | -36.260 | 239.514 | 20.059 |
| 4 | 102.428 | -25.740 | 239.514 | -27.954 | -102.428 | -23.860 | 239.514 | 21.638 |
| 5 | 102.428 | -13.340 | 239.514 | -26.375 | -102.428 | -11.460 | 239.514 | 23.217 |
| 6 | 102.428 | -0.940 | 239.514 | -24.796 | -102.428 | 0.940 | 239.514 | 24.796 |
| 7 | 102.428 | 11.460 | 239.514 | -23.217 | -102.428 | 13.340 | 239.514 | 26.375 |
| 8 | 102.428 | 23.860 | 239.514 | -21.638 | -102.428 | 25.740 | 239.514 | 27.954 |
| 9 | 102.428 | 36.260 | 239.514 | -20.059 | -102.428 | 38.140 | 239.514 | 29.532 |
| 10 | 102.428 | 48.660 | 239.514 | -18.481 | -102.428 | 50.540 | 239.514 | 31.111 |
| 11 | 102.428 | 61.060 | 239.514 | -16.902 | -102.428 | 62.940 | 239.514 | 32.690 |

TABLE 4
COORDINATES OF THE MEASURING POINTS FOR THE PITCH MEASUREMENT

| | X | Y | Z | B |
|---|---|---|---|---|
| Left flank | 0 | -0.940 | 260.497 | 1.642 |
| Right flank | 0 | 0.940 | 260.497 | -1.642 |

TABLE 5
COORDINATES OF THE MEASURING POINTS FOR THE FLANK TOPOGRAPHIC MEASUREMENT

| | Left flank | | | | Right flank | | | |
|---|---|---|---|---|---|---|---|---|
| NO. | X | Y | Z | B | X | Y | Z | B |
| (1,3) | 1.631 | -58.940 | 259.985 | 9.339 | -1.631 | -57.060 | 259.985 | 5.431 |
| (2,3) | 1.631 | -44.440 | 259.985 | 7.493 | -1.631 | -42.560 | 259.985 | 3.585 |
| (3,3) | 1.631 | -29.940 | 259.985 | 5.646 | -1.631 | -28.060 | 259.985 | 1.738 |
| (4,3) | 1.631 | -15.440 | 259.985 | 3.800 | -1.631 | -13.560 | 259.985 | -0.108 |
| (5,3) | 1.631 | -0.940 | 259.985 | 1.954 | -1.631 | 0.940 | 259.985 | -1.954 |
| (6,3) | 1.631 | 13.560 | 259.985 | 0.108 | -1.631 | 15.440 | 259.985 | -3.800 |
| (7,3) | 1.631 | 28.060 | 259.985 | -1.738 | -1.631 | 29.940 | 259.985 | -5.646 |
| (8,3) | 1.631 | 42.560 | 259.985 | -3.585 | -1.631 | 44.440 | 259.985 | -7.493 |
| (9,3) | 1.631 | 57.060 | 259.985 | -5.431 | -1.631 | 58.940 | 259.985 | -9.339 |